Ice-Nucleating Particle Concentrations and Sources in Rainwater over the Third Pole, Tibetan Plateau

J. Chen[1], Z. J. Wu[1,3*], G. M. Wu[2*], X. D. Gong[4#], F. Wang[5], J. C. Chen[1], G. L. Shi[5], M. Hu[1,3], Z. Y. Cong[2]

[1] State Key Joint Laboratory of Environmental Simulation and Pollution Control, College of Environmental Sciences and Engineering, Peking University, Beijing 100871, China.

[2] Key Laboratory of Tibetan Environment Changes and Land Surface Processes, Institute of Tibetan Plateau Research, Chinese Academy of Sciences, Beijing 100101, China.

[3] Collaborative Innovation Center of Atmospheric Environment and Equipment Technology, Nanjing University of Information Science and Technology, Nanjing 210044, China.

[4] Leibniz Institute for Tropospheric Research, Leipzig, 04318, Germany.

[#] Now at: Center for Aerosol Science and Engineering, Department of Energy, Environmental and Chemical Engineering, Washington University in St. Louis, St. Louis, MO, 63130, USA

[5] State Environmental Protection Key Laboratory of Urban Ambient Air Particulate Matter Pollution Prevention and Control, College of Environmental Science and Engineering, Nankai University, Tianjin, 300071, China.

Corresponding author: Zhijun Wu (zhijunwu@pku.edu.cn) and Guangming Wu (wuguangming@itpcas.ac.cn)

Key Points:

- The INP concentrations over the Tibetan Plateau (TP) are comparable to those in Arctic region.
- Biogenic particles are major contributors to INPs at temperatures above -20 ^{o}C.
- Atmospheric INPs over the TP can be impacted by unexpected multi-aerosol sources.

Abstract

The ice-nucleating particles (INPs) modulate the microphysics and radiative properties of clouds. However, less is known concerning their abundance and sources in the most pristine and climatic sensitive regions, such as the Tibetan Plateau (TP). Here, to our best knowledge, we conduct the first investigation on INPs in rainwater collected in the TP region under mixed-phase cloud conditions. The INP concentrations vary from 0.002 to 0.675 L^{-1} Air over the temperature range from -7.1 to -27.5 ^{o}C, being within the INP spectra derived from precipitation under worldwide geophysical conditions, and are also comparable to those in the Arctic region. The heating-sensitive INPs account for 57%±30% of the observed INPs at -20 ^{o}C, and become increasingly important at warmer temperature regime, indicating biogenic particles as major contributors to INPs above -20 ^{o}C over the TP, especially, on the day with additional input of biogenic materials carried by dust particles. Chemical analysis demonstrates the rainwater components are mixture of dust particles, marine aerosol, and anthropogenic pollutants. Dust particles transported from the surrounding deserts and originated from ground surface of TP may contribute to the heating-resistant INPs at temperatures below -20 ^{o}C.

Plain Language Summary

Ice-nucleating particles (INPs) can catalyze the ice crystal formation through heterogeneous ice nucleation, thus play a profound role in the aerosol-cloud interaction. Tibetan Plateau (TP) is one of the most vulnerable climate systems in the word, but we have very less knowledge on INPs over the TP, impeding our understanding of the aerosol-cloud interaction. Here, the INP concentrations and sources are quantified and identified over the TP under conditions relevant to mixed-phase cloud on a basis of comprehensive study on chemical composition and INP properties of rainwater. We found biogenic particles are dominant contributor of INPs at temperatures above -20 ^{o}C. The rainwater chemical components are mixture of dust, marine aerosol, and anthropogenic pollutants. Dust particles may contribute to the heating-resistant INPs in temperatures below -20 ^{o}C. The obvious differences in INP concentrations between TP and the Arctic region are not observed.

1 Introduction

Tibetan Plateau (TP), also known as the third pole, is one of the most pristine and climatic sensitive regions in the earth [*Qiu*, 2008]. Due to its complex terrain and extremely high elevation (~4000 m above the sea level) [*Yao et al.*, 2012], TP has been recognized as a driving force and amplifier for the reginal and global climate change [*Jin et al.*, 2005; *Liu and Chen*, 2000]. Over the last half century, TP has experienced ongoing warming [*Kang et al.*, 2010; *Liu and Chen*, 2000; *Niu et al.*, 2004], with the rate of 0.45°C/decade [*Pepin et al.*, 2015], which is almost double of the global average. The climatic warming over the TP has profound impacts on the global hydrological cycle and climatology, thus gains great concern.

As an integral part of Earth's atmosphere, clouds affect the energy balance of the Earth by absorbing or reflecting the solar and terrestrial radiation. The importance of cloud properties [*Duan and Wu*, 2006; *Hua et al.*, 2018] and aerosol-cloud feedback processes [*Zhao et al.*, 2019] in causing the climatic warming over the TP has been pointed out. Aircraft observations showed that the majority detected clouds in summer were in mixed-phase state and accompanied by active ice processes [*Chang et al.*, 2019]. The cirrus clouds formed through deep convective activities during the Asia monsoon periods were associated with thicker, larger and non-spherical ice crystals in comparison to in situ formed cirrus [*He et al.*, 2019]. Despite the importance of ice-related clouds in climate system over the TP [*Duan and Wu*, 2006; *Hua et al.*, 2018; *Yang et al.*, 2012], the formation mechanism and microphysics of these clouds are still not well presented due to lack of relevant observations.

Primary ice formation in clouds can be initiated by atmospheric ice-nucleating particles (INPs) through heterogeneous ice nucleation. Four pathways have been proposed for the heterogeneous ice nucleation in mixed-phase clouds, and immersion freezing has been widely recognized as the most important ice nucleation mechanism [*Z. A. Kanji et al.*, 2017; *Murray et al.*, 2012]. Therefore, INPs play a key role in affecting the lifetime and radiative properties of clouds. However, compared to the Arctic or Antarctic areas, INPs get much less attention over the TP. To the best of our knowledge, no INP measurement was so far carried out in this region.

Atmospheric aerosols over the TP originate from multi-sources [*Huang et al.*, 2006; *Li et al.*, 2016; *Y Liu et al.*, 2015]. The dust particles from the Taklamakan Desert [*Huang et al.*, 2007; *Ramanathan and Carmichael*, 2008] and the anthropogenic pollutants, such as black carbon (BC) from South Asia and north-western China [*Li et al.*, 2016] could affect the aerosol concentrations and chemical compositions in this region. In addition, TP has diverse natural underlying surfaces including glaciers, lakes and grassland [*Kang et al.*, 2010], which could serve as sources of bioaerosols. As been identified by many laboratory and field studies, dust, biogenic particles and BC were potential INPs to nucleate ice under different conditions [*Hoose and Möhler*, 2012; *Kanji et al.*, 2017; *Murray et al.*, 2012].

Up to now, less is known about the concentrations, sources and the ice nucleation efficiency of INPs, impeding our understanding of cloud formation, and the subsequent precipitation and dissipating process. In this study, INPs in rainwater at temperatures relevant to mixed-phase cloud were detected for the first time in Nam Co, a representative central site over the TP. The possible sources of INPs were furtherly identified by combining the chemical composition and source apportionment analysis.

2 Materials and Methods

2.1 Sampling site and rainwater collection

The Nam Co Station (30.7^{o} N, 90.0^{o} E, 4730 m above sea level) (Fig. S1) for Multisphere Observation and Research locates at central part of the Tibetan Plateau. With very sparse population density and limited anthropogenic atmospheric

pollutants, the average aerosol optical depth (AOD) in Nam Co was 0.05 at the wavelength of 500 nm [*Cong et al.*, 2009] and comparable to that of Arctic [*Pokharel et al.*, 2019]. Therefore, Nam Co represents a clean continental background site. The geophysical characteristic in Nam Co region include mountains, glaciers, lakes, rivers and grassland, which are representative of the main geophysical features over the TP.

A total of 34 rainwater samples was collected at Nam Co Station from January to October in 2018, covering 58.7% of the rainfall events during the sampling period. The detailed sampling information was given in Table S1 in Supporting Information (SI). Samples were collected by disposable Whirl-Pak bags (5L, Nasco, Ft. Wilkinson, Wis.) during each rain event. After the collection, samples were immediately transferred into polycarbonate bottles (Thermo Fisher Scientific MA, USA) and kept frozen at -20 ^{o}C until analysis. The meteorological parameters including air pressure, relative humidity (RH), temperature, wind speed and direction were recorded by an automatic weather station, and were specifically discussed in section 3.1.

2.2 Ice nucleation experiments

A cold-stage based instrument named Peking University Ice Nucleation Array (PKU-INA) was applied for measuring the ice nucleation activity of rainwater samples following the protocol described in *Chen et al.* [2018]. Briefly, for each experiment, 90 droplets from each sample were pipetted onto a hydrophobic glass slide located on the cold stage, and separated by a spacer with 90 compartments. The top of the spacer was sealed by a cover glass to avoid the Wegener-Bergeron-Findeisen process. The cold stage was cooled down to -35 ^{o}C with a cooling rate of 1 ^{o}C/min and monitored by a CCD (charge-coupled device) camera every 6 seconds. The recorded images were analyzed by a MATLAB program to identify the freezing of droplets based on the change of the gray values upon phase transition. Together with the recorded temperature, the number of frozen droplets at each temperature can be determined.

The frozen fraction (f_{ice}) can be defined as Eq. (1):

$$f_{ice} = \frac{N_{frozen}}{N_t} \quad (1)$$

Where N_{frozen} was the number of frozen droplets under certain temperature and N_{t} was the total number of droplets (90 in this study). In the following data reduction and analysis, a time independent freezing of the supercooled droplets was assumed. The cumulative INP number concentrations per water volume ($N_{\mathrm{INP\_water}}$) can be obtained from Eq. (2):

$$N_{\mathrm{INP\_water}} = \frac{-\ln(1-f_{ice})}{V_{drop}} \quad (2)$$

where V_{drop} is the volume of one droplet (1 μl in this study).

Conversion of INP per water volume to INP per air volume ($N_{\mathrm{INP\_air}}$) is achieved by assuming that the cloud condensed water content (CWC) to be 0.15 g m^{-3}, according

to the mean value of the CWC reported over the TP by an aircraft measurement [*Chang et al.*, 2019]. CWC is defined as cloud droplets of 1pL disperse in 1 m^3 of air weigh about 0.15 g, and the corresponding volume of cloud water per volume of air (F_{cloud_air}) was $1.5*10^{-7}$ m^3_{water} m^{-3}_{air} [*Gong et al.*, 2020]. The cumulative number concentration of INPs per unit air (N_{INP_air}) can be obtained from Eq. (3):

$$N_{INP\_air} = F_{cloud\_air} * N_{INP\_water} \quad (3)$$

The estimation of confidence intervals for the number of N_{INP_water} was followed the methods in *Barker* [2002] and *O'Sullivan et al.* [2018], and furtherly used to calculate the confidence intervals for N_{INP_air}. Other uncertainties such as the impacts of dissolved solutes and chemical aging on the INP concentrations of rainwater were pointed out by *Petters and Wright* [2015], which were likely to contribute less than one order of magnitude in INP concentration.

2.3 Chemical analysis and source apportionment

Water-soluble ions (K^+, Mg^{2+}, Ca^{2+}, NH_4^+, NO_3^-, SO_4^{2-} and Cl^-) and water-soluble organic carbon (WSOC) in rainwater were measured by an ion chromatograph (DIONEX, ICS-2500/2000) [*Guo et al.*, 2012] and a TOC analyzer (SHIMADZU, TOC-L CPH CN200), respectively. The Inductively Coupled Plasma-Mass Spectrometry (ICP-MS) (Bruker, aurora M90) was used to determine the metal element concentrations (Na, Mg, Al, K, Ca, Cr, Mn, Fe, Ni, Cu, Zn, Pb and Ba). The mass concentrations of BC in rainwater were measured by a Single Particle Soot Photometer (SP2, Droplet Measurement Technologies, Inc., Boulder, Colorado) [*Kaspari et al.*, 2011; *Stephens et al.*, 2003]. The rainwater was nebulized by a nebulizer (CETAC, U-5000AT, WA, USA) and then introduced into an interaction region, which was created by the jet stream containing BC particles and the intracavity beam emitted from Nd: YAG laser. The peak intensity of incandesce is proportional to the mass concentration of BC. The concentrations of chemical components in rainwater, including water-soluble ions and organic carbon, metal elements and BC were respectively shown in Fig. S2(a) and Fig.S2(b).

The Positive Matrix Factorization Model developed by Environmental Protection Agency (EPA-PMF) [*Norris et al.*, 2014] was performed to identify the sources of chemical components in rainwater on the basis of the measured chemical components. The working principle and the resulting source profile of PMF (Fig.S3) were detailed in Text S1 and Text S2 of SI, respectively. Overall, four sources were identified by PMF model and averagely contribute the following percentage of chemical compounds in rainwater (Fig. S4): dust (14%), marine and salt-lake (27%), long-range transport anthropogenic pollutants (24%) and biomass burning (34%) (Fig.S4), indicating the impacts from diverse aerosol sources over the TP. The contributions of the four identified sources for all samples were displayed in Fig. S5.

2.4 Backward trajectories and Geographic Information System analysis

The 10-day backward trajectories were calculated using the NOAA HYSPLIT (HYbrid Single-Particle Lagrangian Integrated Trajectory) model [*Rolph et al.*, 2017; *Stein et al.*, 2016], with one trajectory related to each sample. Trajectories were in 1-h time resolution and ended at an altitude of 1000 m above the ground level (AGL). The trajectories were then coupled by land cover dataset obtained from Geographic Information System (GIS) to examine which kind of land cover the airmass has passed over before reaching the sampling site. The details of the land cover analysis methodology are given in *Pinxteren et al.* [2010]. During the sampling period, the land cover over which air masses has been passed are categorized into 5 types: water/ice, natural vegetation, agricultural area, urban area and bare area.

3 Results and discussion

3.1 Overview of meteorology

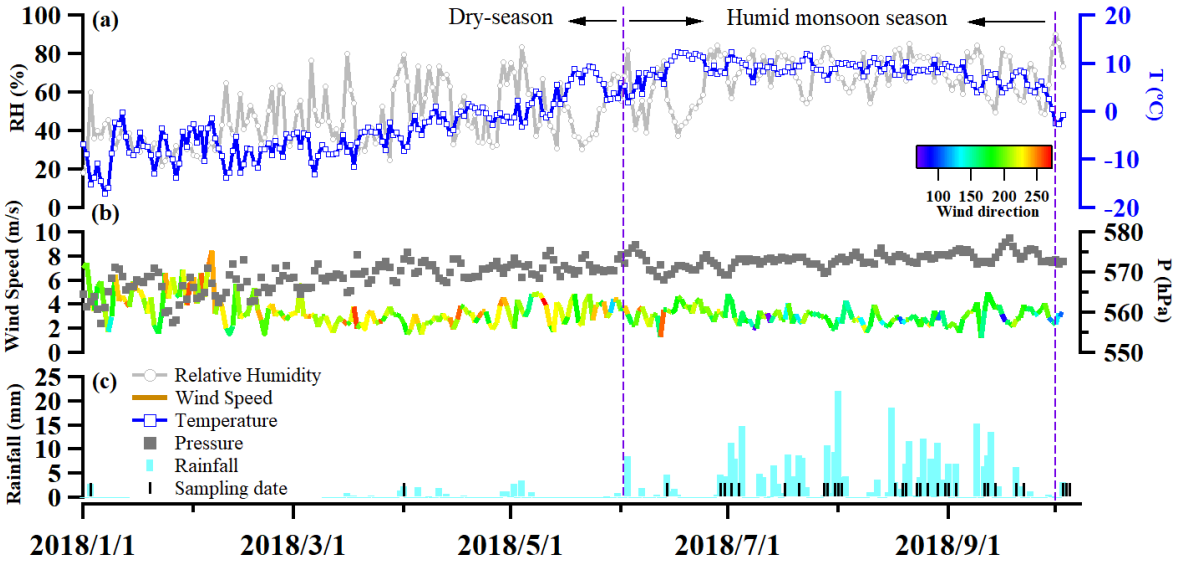

Figure 1. Time series of meteorological parameters including ambient relative humidity (RH) and temperature in panel (a), wind speed/direction and pressure in panel (b), and rainfall in panel (c). The dates on which rainwater was collected were marked by black lines in panel (c).

The time series of the meteorological parameters during the entire sampling period is shown in Fig.1. Over the TP, there are two distinguished seasons, i.e. dry season (October-April) with lower temperature and RH and humid monsoon season (June-September) with higher temperature and RH (Fig. 1(a)). On average, the wind speed was 3.4±1.2 m/s (mean±1 standard deviation), with southernly prevailing wind (See Fig. 1(b) and Fig. S6). Most of precipitation fell in monsoon season under the strong influence of Indian summer monsoon after June (Fig. 1(c)). In dry season, westerlies dominate the large-scale air circulation with less precipitation [*Li et al.*, 2007; *Xu et al.*, 2008] (Fig. 1(c)).

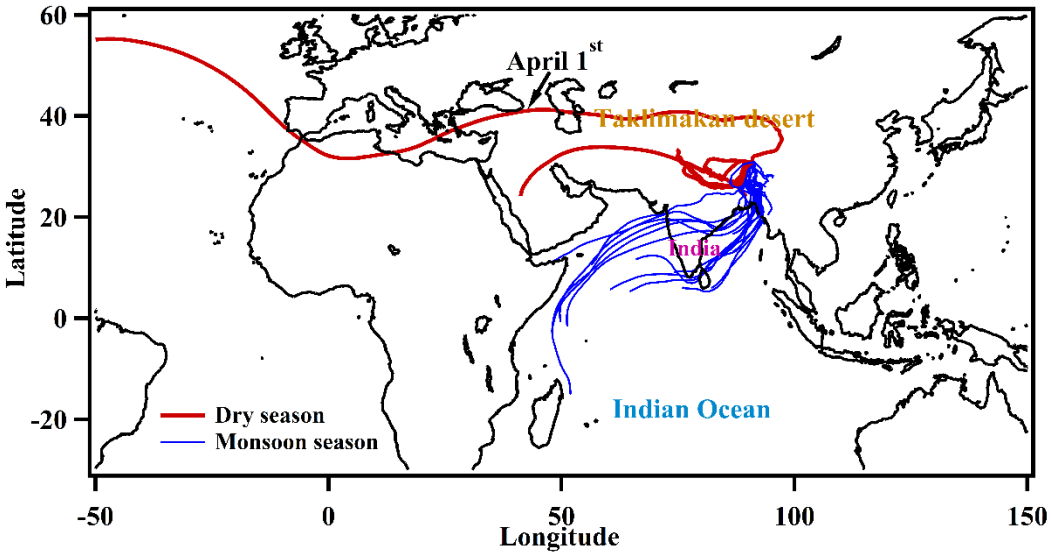

Figure 2. 10-day backward trajectories with 1 h time-resolution ended at 1000 m AGL. Backward trajectories during dry season (January 03rd, April 1st, June 14th, October 3rd, 4th and 5th) and monsoon season (June 14th - September 22nd) are shown in red and blue lines, respectively.

The 10-day backward trajectories were depicted in Fig. 2. Approximately 82% air masses after June 14th originated from Indian ocean, passed over India and Bangladesh, and reached the inland of TP (marked by blue). The rest of six trajectories (marked by red) came from the west or the north. The resulting backward trajectories correspond well to the atmospheric circulation in TP, i.e. air masses were impacted by Indian monsoon and westerlies in humid and dry season, respectively. Therefore, the rainwater samples were categorized into two groups, i.e., monsoon (from June 14th - September 22nd) and dry season samples (others), based on the meteorological conditions and backward trajectory analysis. Notably, the sample collected on April 1st was impacted by the air masses from the north, passing over Taklimakan desert.

The INP concentrations in the rainwater droplets (N_{INP_water}) and cloud air (N_{INP_air}) were depicted in Fig. 3. The N_{INP_air} was derived from $N_{INP\_droplet}$ assuming cloud water content (CWC) of 0.15 g m^{-3} (Eq.3), a mean CWC value of mixed-phase cumulus clouds reported by an aircraft measurement over the TP in summer [*Chang et al.*, 2019]. This CWC value was also consistent with that estimated in precipitating convective clouds over the TP using multiyear satellite observation [*Chen et al.*, 2020]. The N_{INP_air} varied from 0.002 to 0.675 L^{-1} over the temperature range from -7.1 to -27.5 ^{o}C. Most of the observed N_{INP_water} values were within the ranges of INP spectra summarized by *Petters and Wright* [2015] (Fig.3). Exceptions are few measured N_{INP_air} out the lower limitation of the spectra (Fig. S7), but no less than one order of magnitude, due to the lower CWC value reported in TP resulted from high elevation than those obtained in thicker clouds (0.2 and 0.8 g m^{-3}, [*Petters and Wright*, 2015; *Rangno and Hobbs*, 2005]).

246 ### 3.2 Ice-nucleating particle concentrations

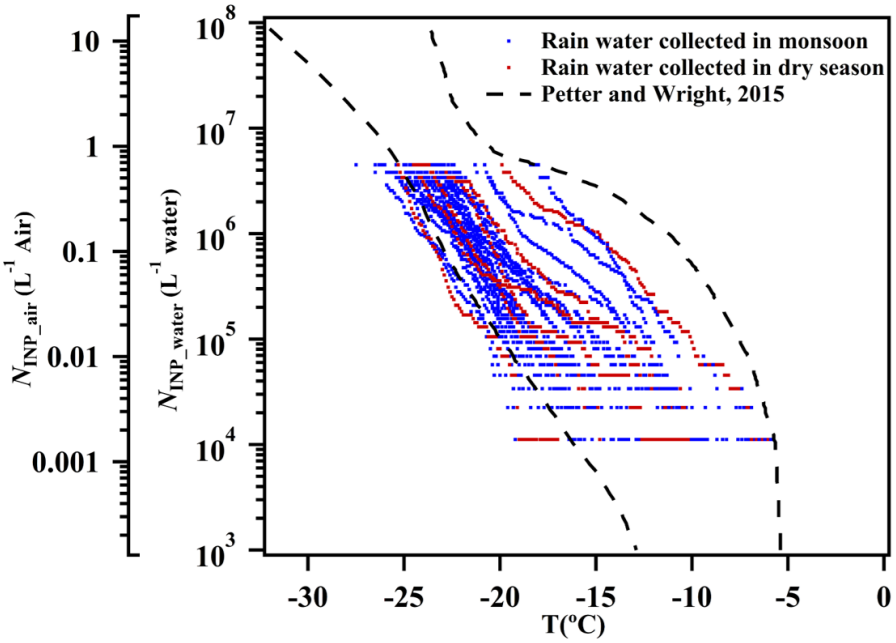

247

248 **Figure 3.** The INP spectra obtained from rainwater in Nam Co in dry (red dots) and
249 monsoon (blue dots) seasons. The enveloped area by two black dashed lines represent
250 the INP concentrations in precipitation samples summarized by *Petters and Wright*
251 [2015]. The first and secondary y axes represent the spectra per volume of water
252 (N_{INP_water}) and the spectra per volume of air (N_{INP_air}) assuming the cloud condensed
253 water content (CWC) of 0.15 g m^{-3} which can be referred to *Chang et al.* [2019].

254 The N_{INP_air} in Nam Co spanned three orders of magnitudes over the
255 determined temperature ranges, indicating a large variety of the INP concentrations
256 observed in different days. Such wide freezing temperature of INPs can be attributed
257 to INPs originated from complex aerosol sources, as verified by source apportionment
258 of rainwater components (Fig.S4). No significant differences of N_{INP} were observed in
259 dry and monsoon seasons (Fig.3), exceptions were one dry season sample (April 1st)
260 and three monsoon samples (August 17th, 30th and 31st) with evidently higher N_{INP}
261 concentrations (>0.2 L^{-1} Air) and onset temperatures (>-10 ^{o}C) (Fig. S7). Already at a
262 first glance, the shape of ice nucleation curves and the higher onset temperatures of
263 these four samples hinted the INPs from biogenic sources (Fig.S7). Details about the
264 origins of INPs for these samples will be furtherly explained in the next section.

265 The comparison of the observed N_{INP_air} at -20 ^{o}C ($N_{INP\_air\text{-}20}$) with those
266 reported in Arctic region was given in Table 1. The maximum discrepancy between
267 $N_{INP\_air\text{-}20}$ over the TP and those in Arctic is only one order of magnitude [*Creamean et*
268 *al.*, 2018; *Hartmann et al.*, 2020; *Irish et al.*, 2019; *Mason et al.*, 2016; *Prenni et al.*,
269 2009; *Si et al.*, 2019; *Tobo et al.*, 2019], indicating comparable $N_{INP\_air\text{-}20}$ in these two
270 pole aeras. As indicated by chemical analysis, the rainwater components came from
271 both natural (mainly marine and dust) and anthropogenic sources (biomass burning
272 and anthropogenic pollutants) (Fig. S4). Resemble to TP, the previous field studies
273 carried out in Arctic region (Table 1), have recognized dust particles [*Creamean et*

al., 2018; *Irish et al.*, 2019; *Tobo et al.*, 2019], marine [*Creamean et al.*, 2018; *Hartmann et al.*, 2020; *Irish et al.*, 2019] and bioaerosols [*Wex et al.*, 2019] as potential INP sources.

Table 1. Comparison of atmospheric N_{INP} at -20 ^{o}C observed over the TP and the Arctic regions.

Site	Time	Particle Size	$N_{INP\_air(-20)}$ (L^{-1})	INP Sources	Reference
Nam Co, Tibetan Plateau	Jan.-Oct., 2018	-	0.11±0.16	Bio, D	This study
High Arctic	Mar.-Apr., 2018	-	<0.1	Bio, M	[*Hartmann et al.*, 2020]
Alert, Ny-Ålesund, Barrow, Svalbard, Villum Research Station	Varied in 2012-2016	-	0.008~0.04	Bio for highly active INPs	[*Wex et al.*, 2019]
Alert, Nunavut, Canada	Spring 2016	< 10 μm	0.020±0.004	D	[*Si et al.*, 2019]
Arctic marine boundary layer	Summer 2014	TSP	0.044	D, M	[*Irish et al.*, 2019]
An outwash plain near Svalbard	Jul., 2016 Mar., 2017	< 5μm	2016:0.02~0.24 2017:0.004~0.02	D	[*Tobo et al.*, 2019]
Alert, Nunavut, Canada	Mar.-May., 2017	TSP	0.22	-	[*Mason et al.*, 2016]
Alaska, Arctic oilfield location	Mar.-Jul., 2014	<12 μm	0.006~0.03	D, M	[*Creamean et al.*, 2018]
Alaska	Oct., 2004	<1.5 μm	0.4	BB, VA	[*Prenni et al.*, 2009]

*D refer as dust aerosol; M refer as marine aerosol; BB refer as biomass burning aerosol; Bio refer as biogenic aerosol; VA refer as volcanic ash; TSP refer as total suspended particulate

3.3 Contribution of biogenic ice-nucleating particles

INPs being sensitive to heat were inferred as protein-based biogenic INPs [*Christner et al.*, 2008b]. Thus, to quantify the concentrations of biogenic INPs in rainwater, the experiments with samples being heated to 95^{o}C for 10 minutes were conducted (refer to *Joly et al.* [2014]). Figure 4 depicts the reduction ratio of N_{INP_air} at different temperatures (-15 ^{o}C, -18 ^{o}C, -20 ^{o}C and -22 ^{o}C). On average, the reduction of N_{INP_-15} due to heat was 84%±17% (mean ± standard deviation), indicating a large fraction of the observed INPs at -15 ^{o}C were in biogenic origin. The reduction ratio down to 57%±30% (mean ± standard deviation) at -20 ^{o}C, as expected, the lower contribution from biogenic INPs with decreased freezing temperatures. Such results indicate the prevalence of biogenic INPs in the rainwater and these INPs would become more important in higher temperatures [*Christner et al.*, 2008a; *Christner et al.*, 2008b; *Gong et al.*, 2020; *Hill et al.*, 2014; *Joly et al.*, 2014; *Stopelli et al.*, 2014]

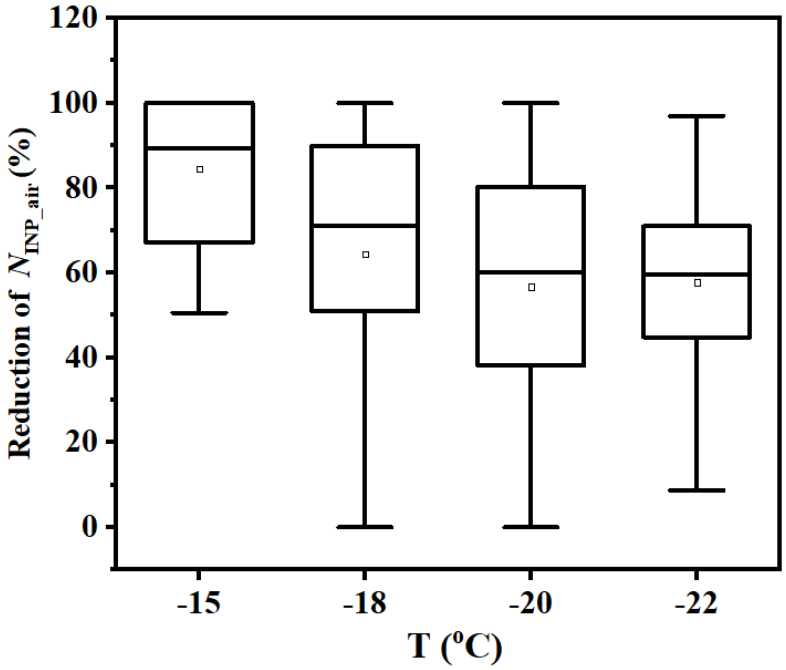

Figure 4. Boxplot of the reduction ratio of N_{INP_air} at different temperatures (-15 ^{o}C, -18 ^{o}C, -20 ^{o}C and -22 ^{o}C) after being heated to 95 ^{o}C for 10 minutes. The boxes represent the interquartile range. The whiskers represent the 10th and 90th percentiles. The squares represent the mean values.

Moreover, the reduction ratio kept constant at temperatures below -20 ^{o}C, for example, a value of 57%±30% (mean ± standard deviation) and 58±22% (mean ± standard deviation) was observed at 20 ^{o}C and -22 ^{o}C, respectively. This can also be seen in Fig. S8, the elimination of N_{INP_air} after being heated mainly occurred at temperatures warmer than -20 ^{o}C. The combined results indicate the INPs in biogenic origin dominated the N_{INP_air} at temperatures above -20 ^{o}C, while the heating-resistant INPs become more important at temperatures below -20 ^{o}C.

Figure 5 exemplarily illustrates the N_{INP_air} at -18 ^{o}C ($N_{INP\_air(-18)}$) in rainwater, comprised of heating-sensitive biogenic INPs (biogenic $N_{INP\_air(-18)}$) and heating-resistant INPs (HR-$N_{INP\_air(-18)}$). We note that heat lead to a significant reduction in INPs (~86%) at -18 ^{o}C for the above-mentioned four samples (April 1st, August 17th, 30th and 31st) with unusual high INP concentrations (Fig. 5), implying the bioaerosols elevated N_{INP_air} in these samples to extremely high level.

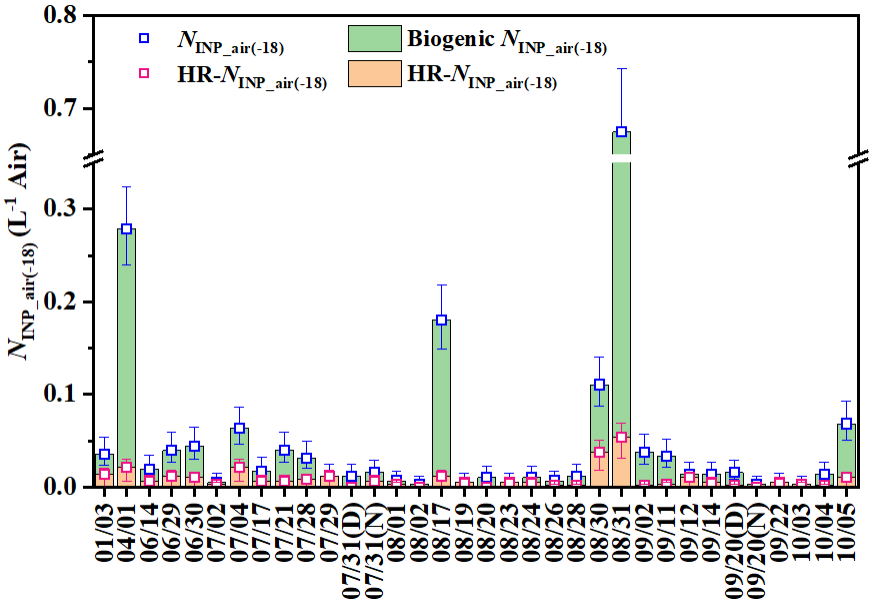

Figure 5. The INP concentrations at -18 °C ($N_{INP\_air(-18)}$, blue squares), comprised of heating-sensitive biogenic (green bars) and heating-resistant (orange bars and red squares) INPs. The error bars represent the confidence interval of 95%. D and N refer as the samples collected during daytime and nighttime in the same day.

One interesting thing is that the rainwater collected on April 1st showed obvious signs from dust particles. The air mass backward trajectory on this day passed over the northern Taklimakan desert (Fig.2) and spent a large percentage of time over bare areas (Fig.S9). Enriched crustal elements (Ca, Mg, Al and Fe), 9 times higher than average, were detected accordingly (Fig. S2(b)). The strong influences of dust can also be seen from source apportionment (Fig. S5). As we know, dust particles can solely act as INPs at temperatures below -20 °C [*Kanji et al.*, 2017] or become ice active in warmer temperature by carrying ice-active biogenic macromolecules [*Conen et al.*, 2011; *O'Sullivan et al.*, 2016]. Thus, biogenic materials carried by dust particles bring additional heating-sensitive biogenic INPs, as a result, lead to the improvement of ice nucleating activities of dust particles and high INP concentration on April 1st.

Backward trajectories and Geographic Information System (GIS) analysis showed that the air masses averagely spent considerable time over the natural vegetation (54.3%) and agricultural areas (32.2%), but less time over water/ice (10.8%), bare (2.6%) and urban (0.1%) aeras during the sampling period (Fig. S9). The agricultural soil [*Conen et al.*, 2011; *O'sullivan et al.*, 2014] was found to contribute to the atmospheric biogenic INPs. So, the long residence time of air masses over natural vegetation and agricultural areas, indicating such underlying surfaces can priorly serve as sources of biogenic INPs. While the water/ice surface may not contribute to the INPs significantly, due to limited residence time and low ice nucleating efficiency of INPs when air mass passed over the open water and ice [*Gong et al.*, 2020; *Irish et al.*, 2019; *Si et al.*, 2019]. The source apportionment based on chemical compositions of rainwater on July 29th and August 26th showed strong

impacts from marine and salt-lake sources (Fig. S5), but these days were not associated with high biogenic or total $N_{INP\_air(-18)}$ (Fig. 5). Thus, bioaerosols from continental source were more likely to be major contributor of the INPs and resulted in the elevation of INPs other than those from the open water source (marine and salt-lake source).

3.4 Ice-nucleating particles from abiotic sources

As shown in Fig. 4, the HR-N_{INP_air} became more important with the decreasing temperature. The contribution of HR-N_{INP_air} to total N_{INP_air} reached up to 40% at temperatures below -20 ^{o}C. The chemical composition analysis showed that almost all the detected samples consisted of crustal elements (Ca, Mg, Al and Fe) (Fig.S2), indicating the presence of dust materials in rainwater. The effects of dust particles on rain samples can also be confirmed by source apportionment (Fig.S4). The observed heating-resistant INPs in this study were found to dominate the ice nucleation in rainwater at temperatures below -20 ^{o}C (Fig. 4 and Fig. S8), being consistent with the typical activated temperatures for dust particles [*Kanji et al.*, 2017]. The surrounding deserts and the ground surface over the TP can be the sources of dust particles [*Kang et al.*, 2016; *Pokharel et al.*, 2019], contributing to the observed HR-N_{INP_air} in rainwater.

BC, another heating-resistant material, was found in the rainwater samples. Its mean concentration in the detected rainwater was 1.07±1.05 ng/ml. BC may come from South Asia with intensive biomass burning and fossil fuel combustion via the the long-range transport [*Li et al.*, 2016]. This was evidenced by the source apportionment (Fig.S9). Assuming the CWC of 0.15 g m^{-3}, the mean value of BC concentration in per volume of air was 0.16±0.16 ng/m^3, which was remarkably lower than the mean values reported in two of our previous work (3200 and 7700 ng/m^3) in urban areas in China [*Chen et al.*, 2018; *Gong et al.*, 2016]. No obvious correlation between HR-N_{INP_air} and BC mass concentration was found (R^2=0.087), consistent with the INP measurement in Beijing showing no correlation between BC mass concentration and N_{INP_air} at temperatures above -25 ^{o}C [*Chen et al.*, 2018].In addition, most of the studies showed inefficient ice nucleating activities of BC over the temperature ranges relevant for mixed-phase clouds [*Chou et al.*, 2013; *Kanji et al.*, 2020; *Mahrt et al.*, 2018; *Schill et al.*, 2020; *Vergara-Temprado et al.*, 2018]. Combined with these results, we suggest the BC generated from biomass burning and fossil fuel combustion may play a minor role in the INPs in rainwater over the TP due to low concentration and poor ice nucleating activities.

4 Conclusions

The abundance and the potential sources of atmospheric ice-nucleating particles (INPs) at central Tibetan Plateau (i.e., Nam Co) are quantified and identified by coupling detailed chemical composition analysis and INP measurements of rainwater samples. The observed INP concentrations varied from 0.002 to 0.675 L^{-1} over the temperature range from -7.1 ^{o}C to -27.5 ^{o}C, being within the range of INP spectra

derived by *Petters and Wright* [2015] and were comparable to those measured in the Arctic region.

Heating experiments demonstrate that the biogenic INPs averagely accounted for 57%±30% (mean ± standard deviation) of the total INPs at -20 ^{o}C and became even more important at warmer temperature regime. The continental underlying surfaces over the TP, such as natural vegetation and agricultural areas could priorly serve as sources of these biogenic INPs. Chemical analysis showed the rainwater components may be influenced by mixed sources including dust particles, marine aerosols, and anthropogenic pollutants. The components associating with dust particles either transported from surrounding deserts or originated from the ground surface over the TP can contribute to the heating-resistant INPs at temperatures below -20 ^{o}C. BC in rainwater, with the mean concentration of 1.07±1.05 ng/ml, may come from South Asia with intensive biomass burning and anthropogenic activities via long-range transport. Due to much lower content and inefficient ice nucleating activities in the determined temperature range, BC may not be responsible for the observed heating-resistant INPs.

Our work indicates the rainwater components collected in TP are impacted by unexpected multi-aerosol sources. As a result, the variations and properties of INPs are modulated by both natural and anthropogenic aerosols. Currently, the limited studies are unable to provide a full picture of INPs over the third pole regions. Thus, we suggest more INP measurements are required in this region to parse out the sources and seasonal characteristics of INPs, which would be of great help to improve our understanding of the aerosol-cloud interaction and climate change in the third pole region.

Acknowledgments

This work is supported by the following projects: National Natural Science Foundation of China (4191101414, 41875149 and 91844301). We gratefully acknowledge the Dr. Dominik van Pinxteren in Leibniz Institute for Tropospheric Research for the land cover analysis. And we also thank Dr. Yutaka Tobo in National Institute of Polar Research in Japan and Dr. Heike Wex in Leibniz Institute for Tropospheric Research for offering their INP dataset in Arctic region.

Data Availability

The archiving of data that support the collusion of this work is under way. We plan to upload our dataset to PANGAEA® Data publisher. The dataset is temporarily described in the Supplementary Information.

References

Barker, L. (2002), A comparison of nine confidence intervals for a Poisson parameter when the expected number of events is≤5, *Am. Stat.*, *56*(2), 85-89.

Chang, Y., X. Guo, J. Tang, and G. Lu (2019), Aircraft measurement campaign on summer cloud microphysical properties over the Tibetan Plateau, *Sci. Rep.*, *9*(1), 4912.

Chen, J., X. Wu, Y. Yin, and C. Lu (2020), Large-Scale Circulation Environment and

Microphysical Characteristics of the Cloud Systems Over the Tibetan Plateau in Boreal Summer, *Earth. Space. Sci.*, *7*(5), e2020EA001154.

Chen, J., X. Pei, H. Wang, J. Chen, Y. Zhu, M. Tang, and Z. Wu (2018), Development, Characterization, and Validation of a Cold Stage-Based Ice Nucleation Array (PKU-INA), *Atmosphere*, *9*(9), 357.

Chen, J., Z. Wu, S. Augustin-Bauditz, S. Grawe, M. Hartmann, X. Pei, Z. Liu, D. Ji, and H. Wex (2018), Ice-nucleating particle concentrations unaffected by urban air pollution in Beijing, China, *Atmos. Chem. Phys.*, *18*(5), 3523-3539.

Chou, C., Z. Kanji, O. Stetzer, T. Tritscher, R. Chirico, M. Heringa, E. Weingartner, A. Prévôt, U. Baltensperger, and U. Lohmann (2013), Effect of photochemical ageing on the ice nucleation properties of diesel and wood burning particles, *Atmos. Chem. Phys.*, *13*(2), 761.

Christner, B. C., C. E. Morris, C. M. Foreman, R. Cai, and D. C. Sands (2008a), Ubiquity of biological ice nucleators in snowfall, *Science*, *319*(5867), 1214-1214.

Christner, B. C., R. Cai, C. E. Morris, K. S. McCarter, C. M. Foreman, M. L. Skidmore, S. N. Montross, and D. C. Sands (2008b), Geographic, seasonal, and precipitation chemistry influence on the abundance and activity of biological ice nucleators in rain and snow, *P. Natl. Acad. Sci. USA.*, *105*(48), 18854-18859.

Conen, F., C. Morris, J. Leifeld, M. Yakutin, and C. Alewell (2011), Biological residues define the ice nucleation properties of soil dust, *Atmos. Chem. Phys.*, *11*(18), 9643-9648.

Cong, Z., S. Kang, A. Smirnov, and B. Holben (2009), Aerosol optical properties at Nam Co, a remote site in central Tibetan Plateau, *Atmos. Res.*, *92*(1), 42-48.

Creamean, J. M., R. M. Kirpes, K. A. Pratt, N. J. Spada, M. Maahn, G. de Boer, R. C. Schnell, and S. China (2018), Marine and terrestrial influences on ice nucleating particles during continuous springtime measurements in an Arctic oilfield location, *Atmos. Chem. Phys.*, *18*(24), 18023-18042.

Duan, A., and G. Wu (2006), Change of cloud amount and the climate warming on the Tibetan Plateau, *Geophys. Res. Lett.*, *33*(22).

Gong, X., C. Zhang, H. Chen, S. A. Nizkorodov, J. Chen, and X. Yang (2016), Size distribution and mixing state of black carbon particles during a heavy air pollution episode in Shanghai, *Atmos. Chem. Phys.*, *16*(8), 5399-5411.

Gong, X., et al. (2020), Characterization of aerosol particles at Cabo Verde close to sea level and at the cloud level - Part 2: Ice-nucleating particles in air, cloud and seawater, *Atmos. Chem. Phys.*, *20*(3), 1451-1468.

Guo, S., M. Hu, Q. Guo, X. Zhang, M. Zheng, J. Zheng, C. C. Chang, J. J. Schauer, and R. Zhang (2012), Primary sources and secondary formation of organic aerosols in Beijing, China, *Environ. Sci. Technol.*, *46*(18), 9846-9853.

Hartmann, M., et al. (2020), Wintertime Airborne Measurements of Ice Nucleating Particles in the High Arctic: A Hint to a Marine, Biogenic Source for Ice Nucleating Particles, *Geophys. Res. Lett.*, *47*(13), e2020GL087770.

He, Q., X. Zheng, J. Li, W. Gao, Y. Wang, T. Cheng, J. Pu, J. Liu, and C. Li (2019), The role of ASM on the formation and properties of cirrus clouds over the Tibetan Plateau, *Tellus B.*, *71*(1), 1577070.

Hill, T. C., B. F. Moffett, P. J. DeMott, D. G. Georgakopoulos, W. L. Stump, and G. D. Franc (2014), Measurement of ice nucleation-active bacteria on plants and in precipitation by quantitative PCR, *Appl. Environ. Microbiol.*, *80*(4), 1256-1267.

Hoose, C., and O. Möhler (2012), Heterogeneous ice nucleation on atmospheric aerosols: a review of results from laboratory experiments, *Atmos. Chem. Phys.*, *12*(20), 9817-9854.

Hua, S., Y. Liu, R. Jia, S. Chang, C. Wu, Q. Zhu, T. Shao, and B. Wang (2018), Role of clouds in accelerating cold-season warming during 2000–2015 over the Tibetan Plateau, *Int. J. Climatol.*, *38*(13), 4950-4966.

Huang, J., B. Lin, P. Minnis, T. Wang, X. Wang, Y. Hu, Y. Yi, and J. K. Ayers (2006), Satellite-based assessment of possible dust aerosols semi-direct effect on cloud water path over East Asia, *Geophys. Res. Lett.*, *33*(19).

Huang, J., P. Minnis, Y. Yi, Q. Tang, X. Wang, Y. Hu, Z. Liu, K. Ayers, C. Trepte, and D. Winker (2007), Summer dust aerosols detected from CALIPSO over the Tibetan Plateau, *Geophys. Res. Lett.*, *34*(18).

Irish, V. E., et al. (2019), Ice nucleating particles in the marine boundary layer in the Canadian Arctic during summer 2014, *Atmos. Chem. Phys.*, *19*(2), 1027-1039.

Jin, L., A. Ganopolski, F. Chen, M. Claussen, and H. Wang (2005), Impacts of snow and glaciers over Tibetan Plateau on Holocene climate change: Sensitivity experiments with a coupled model of intermediate complexity, *Geophys. Res. Lett.*, *32*(17).

Joly, M., P. Amato, L. Deguillaume, M. Monier, C. Hoose, and A.-M. Delort (2014), Quantification of ice nuclei active at near 0 C temperatures in low-altitude clouds at the Puy de Dôme atmospheric station, *Atmos. Chem. Phys.*, *14*(15), 8185-8195.

Kang, L., J. Huang, S. Chen, and X. Wang (2016), Long-term trends of dust events over Tibetan Plateau during 1961–2010, *Atmos. Environ.*, *125*, 188-198.

Kang, S., Y. Xu, Q. You, W.-A. Flügel, N. Pepin, and T. Yao (2010), Review of climate and cryospheric change in the Tibetan Plateau, *Environ. Res. Lett.*, *5*(1), 015101.

Kanji, Z. A., A. Welti, J. C. Corbin, and A. A. Mensah (2020), Black Carbon Particles Do Not Matter for Immersion Mode Ice Nucleation, *Geophys. Res. Lett.*, *47*(11), e2019GL086764.

Kanji, Z. A., L. A. Ladino, H. Wex, Y. Boose, M. Burkert-Kohn, D. J. Cziczo, and M. Krämer (2017), Chapter 1: overview of ice nucleating particles, *Meteor. Monogr.*, *58*, 1.1-1.33.

Kaspari, S. D., M. Schwikowski, M. Gysel, M. G. Flanner, S. Kang, S. Hou, and P. A. Mayewski (2011), Recent increase in black carbon concentrations from a Mt. Everest ice core spanning 1860–2000 AD, *Geophys. Res. Lett.*, *38*(4).

Li, C., S. Kang, Q. Zhang, and S. Kaspari (2007), Major ionic composition of precipitation in the Nam Co region, Central Tibetan Plateau, *Atmos. Res.*, *85*(3-4), 351-360.

Li, C., C. Bosch, S. Kang, A. Andersson, P. Chen, Q. Zhang, Z. Cong, B. Chen, D. Qin, and Ö. Gustafsson (2016), Sources of black carbon to the Himalayan–Tibetan Plateau glaciers, *Nat. Commun.*, *7*(1), 1-7.

Liu, X., and B. Chen (2000), Climatic warming in the Tibetan Plateau during recent decades, *Nt. J. Climatol.*, *20*(14), 1729-1742.

Liu, Y., Y. Sato, R. Jia, Y. Xie, J. Huang, and T. Nakajima (2015), Modeling study on the transport of summer dust and anthropogenic aerosols over the Tibetan Plateau, *Atmos. Chem. Phys.*, *15*(21), 12581-12594.

Mahrt, F., C. Marcolli, R. O. David, P. Grönquist, E. J. Barthazy Meier, U. Lohmann, and Z. A. Kanji (2018), Ice nucleation abilities of soot particles determined with the Horizontal Ice Nucleation Chamber, *Atmos. Chem. Phys.*, *18*(18), 13363-13392.

Mason, R., M. Si, C. Chou, V. Irish, R. Dickie, P. Elizondo, R. Wong, M. Brintnell, M. Elsasser,

511 and W. Lassar (2016), Size-resolved measurements of ice-nucleating particles at six locations in North
512 America and one in Europe, *Atmos. Chem. Phys.*, *16*(3), 1637-1651.
513 Murray, B. J., D. O'Sullivan, J. D. Atkinson, and M. E. Webb (2012), Ice nucleation by particles
514 immersed in supercooled cloud droplets, *Chem. Soc. Rev.*, *41*(19), 6519-6554.
515 Niu, T., L. Chen, and Z. Zhou (2004), The characteristics of climate change over the Tibetan
516 Plateau in the last 40 years and the detection of climatic jumps, *Adv. Atmos. Sci.*, *21*(2), 193-203.
517 Norris, G., Duvall, R., Brown, S., and Bai, S.: EPA Positive Matrix Factorization (PMF) 5.0
518 Fundamentals and User Guide, 2014.
519 O'Sullivan, D., B. J. Murray, J. F. Ross, and M. E. Webb (2016), The adsorption of fungal
520 ice-nucleating proteins on mineral dusts: a terrestrial reservoir of atmospheric ice-nucleating particles,
521 *Atmos. Chem. Phys.*, *16*(12), 7879-7887.
522 O'sullivan, D., B. Murray, T. Malkin, T. Whale, N. Umo, J. Atkinson, H. Price, K. Baustian, and
523 M. Webb (2014), Ice nucleation by fertile soil dusts: relative importance of mineral and biogenic
524 components, *Atmos. Chem. Phys.*, *14*(4), 1853-1867.
525 O'Sullivan, D., M. P. Adams, M. D. Tarn, A. D. Harrison, J. Vergara-Temprado, G. Porter, M. A.
526 Holden, A. Sanchez-Marroquin, F. Carotenuto, and T. F. Whale (2018), Contributions of biogenic
527 material to the atmospheric ice-nucleating particle population in North Western Europe, *Sci. Rep.*, *8*(1),
528 13821.
529 Pepin, N., et al. (2015), Elevation-dependent warming in mountain regions of the world, *Nat. Clim.*
530 *Change.*, *5*(5), 424-430.
531 Petters, M. D., and T. P. Wright (2015), Revisiting ice nucleation from precipitation samples,
532 *Geophys. Res. Lett.*, *42*(20), 8758-8766.
533 Pokharel, M., et al. (2019), Aerosol Properties Over Tibetan Plateau From a Decade of
534 AERONET Measurements: Baseline, Types, and Influencing Factors, *J. Geophys. Res.*, *124*(23),
535 13357-13374.
536 Prenni, A. J., P. J. Demott, D. C. Rogers, S. M. Kreidenweis, G. M. Mcfarquhar, G. Zhang, and M.
537 R. Poellot (2009), Ice nuclei characteristics from M-PACE and their relation to ice formation in clouds,
538 *Tellus B: Chemical and Physical Meteorology*, *61*(2), 436-448.
539 Qiu, J. (2008), China: the third pole, in *Nature*, edited, pp. 393-396.
540 Ramanathan, V., and G. Carmichael (2008), Global and regional climate changes due to black
541 carbon, *Nat. Geosci.*, *1*(4), 221-227.
542 Rangno, A. L., and P. V. Hobbs (2005), Microstructures and precipitation development in
543 cumulus and small cumulonimbus clouds over the warm pool of the tropical Pacific Ocean, *Q. J. Roy.*
544 *Meteor. Soc.*, *131*(606), 639-673.
545 Rolph, G., A. Stein, and B. Stunder (2017), Real-time Environmental Applications and Display
546 sYstem: READY, *Envrion. Modell. Softw.*, *95*, 210-228.
547 Schill, G. P., et al. (2020), The contribution of black carbon to global ice nucleating particle
548 concentrations relevant to mixed-phase clouds, *P. Natl. Acad. Sci. USA.*, 202001674.
549 Si, M., et al. (2019), Concentrations, composition, and sources of ice-nucleating particles in the
550 Canadian High Arctic during spring 2016, *Atmos. Chem. Phys.*, *19*(5), 3007-3024.
551 Stein, A. F., R. R. Draxler, G. D. Rolph, B. J. B. Stunder, M. D. Cohen, and F. Ngan (2016),
552 NOAA's HYSPLIT Atmospheric Transport and Dispersion Modeling System, *B. Am. Meteorol. Soc.*,
553 *96*(12), 2059-2077.
554 Stephens, M., N. Turner, and J. Sandberg (2003), Particle identification by laser-induced

555 incandescence in a solid-state laser cavity, *Applied optics*, *42*(19), 3726-3736.
556 Stopelli, E., F. Conen, L. Zimmermann, C. Alewell, and C. E. Morris (2014), Freezing nucleation
557 apparatus puts new slant on study of biological ice nucleators in precipitation, *Atmos. Meas. Tech.*, *7*(1),
558 129-134.
559 Tobo, Y., et al. (2019), Glacially sourced dust as a potentially significant source of ice nucleating
560 particles, *Nat. Geosci.*, *12*(4), 253-258.
561 Van Pinxteren, D., E. Brüggemann, T. Gnauk, K. Müller, C. Thiel, and H. Herrmann (2010), A
562 GIS based approach to back trajectory analysis for the source apportionment of aerosol constituents
563 and its first application, *J. Atmos. Chem.*, *67*(1), 1.
564 Vergara-Temprado, J., et al. (2018), Is Black Carbon an Unimportant Ice-Nucleating Particle in
565 Mixed-Phase Clouds?, *J. Geophys. Res.*, *123*(8), 4273-4283.
566 Wex, H., et al. (2019), Annual variability of ice-nucleating particle concentrations at different
567 Arctic locations, *Atmos. Chem. Phys.*, *19*(7), 5293-5311.
568 Xu, Z., T. Gong, and J. Li (2008), Decadal trend of climate in the Tibetan Plateau-regional
569 temperature and precipitation, *Hydrol. Process.*, *22*(16), 3056-3065.
570 Yang, K., B. Ding, J. Qin, W. Tang, N. Lu, and C. Lin (2012), Can aerosol loading explain the
571 solar dimming over the Tibetan Plateau?, *Geophys. Res. Lett.*, *39*(20).
572 Yao, T., L. G. Thompson, V. Mosbrugger, F. Zhang, Y. Ma, T. Luo, B. Xu, X. Yang, D. R.
573 Joswiak, and W. Wang (2012), Third pole environment (TPE), *Environ. Dev.*, *3*, 52-64.
574 Zhao, C., Y. Yang, H. Fan, J. Huang, Y. Fu, X. Zhang, S. Kang, Z. Cong, H. Letu, and M.
575 Menenti (2019), Aerosol characteristics and impacts on weather and climate over the Tibetan Plateau,
576 *Natl. Sci. Rev.*